

Hydration-induced softening of the Si-O bonds in olivine

Jingui Xu^{1, 2}, Dawei Fan¹, Dongzhou Zhang², Bo Li^{1, 3}, Wenge Zhou¹ and Przemyslaw K. Dera²

¹Key Laboratory for High-Temperature and High-Pressure Study of the Earth's Interior, Institute of Geochemistry, Chinese Academy of Sciences, Guiyang 550081, China.

²Hawai'i Institute of Geophysics and Planetology, School of Ocean and Earth Science and Technology, University of Hawai'i at Manoa, Honolulu, Hawaii 96822, United States.

³University of Chinese Academy of Sciences, Beijing, 100049, China.

Abstract

Incorporation of hydrogen as OH^- in olivine has been the focus of intense interest in mineral sciences due to its importance for mantle dynamics. Generally, two hydration mechanisms associated with the M and Si sites have been identified in olivine. It is thus important to understand the effects of each of these hydration mechanisms on the high-pressure structural evolution of olivine. Here, we synthesized hydrous Mg-rich olivine (Fo₉₅; 1538 ppm water) at low SiO₂ activity, and identified that the incorporated hydrogens are predominantly associated with the Si sites. HP single-crystal X-ray diffraction (SCXRD) experiments on this olivine revealed a hydration-induced compression behavior change at \sim 20 GPa by softening of the Si-O bonds. This anomaly in the compression anisotropy could be expected in cold subducting slabs where a large volume of metastable olivine exists and could contribute to the seismic anisotropy of the slabs.

1. Introduction

Mg-rich olivine is the dominant mineral of the Earth's upper mantle and constitutes up to \sim 60% of mantle rock by volume, based on a pyrolite model (Ita & Stixrude, 1992). Understanding the stability and elasticity of olivine at elevated pressure and temperature is important for modeling the structure of the Earth's interior. Under normal mantle geotherm, the $\alpha \rightarrow \beta \rightarrow \gamma$ phase transitions of Mg-rich olivine have been considered to be responsible for the seismic discontinuities at depths around 410 and 520 km (Ringwood, 1991). In subduction zones, the internal cold conditions of subducting slabs allow olivine to metastably survive to the transition zone, and the anticrack faulting associated with the metastable phase transitions has been proposed as a possible mechanism of deep Earthquake generation (Kirby et al., 1991; Kirby et al., 1996).

Due to its geological importance, Mg-rich olivine has been extensively studied at high-pressure conditions (e.g., Hazen, 1976; Kudoh & Takéuchi, 1985; Will et al., 1986; Andrault et al., 1995; Duffy et al., 1995; Downs et al., 1996; Zha et al., 1996; Zha et al., 1998; Rouquette et al., 2008; Nestola et al., 2011; Finkelstein et al., 2014; Mao et al., 2015; Santamaria-Perez et al., 2016). At ambient temperature, Mg-rich olivine metastably retains its structure to \sim 50 GPa under quasi-hydrostatic compression (Finkelstein et al., 2014; Santamaria-Perez et al., 2016). HP single-crystal X-ray diffraction (SCXRD) experiments revealed that Mg-endmember olivine (Fo-forsterite; Mg_2SiO_4) undergoes two HP phase transitions $\text{Fo} \rightarrow \text{FoII}$ and $\text{FoII} \rightarrow \text{FoIII}$ at \sim 50 and \sim 58 GPa, respectively (Finkelstein et al., 2014). Utilizing HP Raman spectroscopy (RS), similar phase transitions have also been confirmed in natural San Carlos olivine (Fo₉₀) at similar transition pressures (Santamaria-Perez et al., 2016). The compression of olivine is continuous until the phase transition, as indicated by the variations of its unit cell parameters and frequencies of Raman vibrational modes with increasing pressure (Hazen, 1976; Downs et al., 1996; Liu & Li, 2006; Nestola et al., 2011; Finkelstein et al., 2014; Santamaria-Perez et al., 2016).

Another topic that has generated broad interest in geophysics and geochemistry is the incorporation of hydrogen into olivine. Natural mantle-derived olivine typically contains tens to hundreds of ppm of water by weight (e.g., Bell & Rossman, 1992; Beran & Libowitzky, 2006), however, HP experiments have suggested that the water solubility in olivine is controlled by several parameters including pressure, temperature, oxygen and water fugacity, and silica activity (e.g., Kohlstedt et al., 1996; Mosenfelder et al., 2006; Smyth et al., 2006) and the

maximum can be as high as 8900 ppm (Smyth et al., 2006). Generally, there are two different groups of the mechanism by which hydrogen is incorporated in the olivine structure. Group I is associated with the Si site, and group II is dominated by the M site (Kohlstedt et al., 1996; Lemaire et al., 2004; Berry et al., 2005; Berry et al., 2007; Walker et al., 2007). In a Fourier transform infrared spectroscopy (FTIR) spectrum, absorption bands of group I are located between 3450 and 3650 cm^{-1} , while those of group II are at 3200-3450 cm^{-1} (Kohlstedt et al., 1996; Berry et al., 2005; Berry et al., 2007). The incorporation of water can have dramatic effects on the stability and elasticity of minerals (e.g., Litasov et al., 2005; Jacobsen, 2006; Frost & Dolejš, 2007; Fan et al., 2017). As a result, a number of studies have been conducted on the effects of water on the phase transition and elasticity of olivine (e.g., Jacobsen et al., 2008; Mao et al., 2010; Chen et al., 2011; Ghosh et al., 2013; Manghnani et al., 2013).

Water decreases the pressure of the $\alpha \rightarrow \beta$ phase transition of olivine (Frost & Dolejš, 2007) and increases the pressure of the post-spinel transition (Litasov et al., 2005; Ghosh et al., 2013). Water also significantly decreases the bulk modulus of olivine (e.g., Jacobsen, 2006; Jacobsen et al., 2008; Manghnani et al., 2013; Mao & Li, 2016). Compared to anhydrous olivine (Mao et al., 1970; Liu, 1975; Durben et al., 1993; Liu & Mernagh, 1993; Andrault et al., 1995; Downs et al., 1996; Zhang, 1998; Rouquette et al., 2008; Finkelstein et al., 2014; Zhang, Hu, et al., 2017; Zhang et al., 2019), HP studies on the metastable phase transitions in hydrous olivine are relatively limited (Manghnani et al., 2013). At ambient temperature, HP powder X-ray diffraction (PXRD) experiments revealed that Fo_{97} containing 4883 ppm water retains its structure to ~ 34 GPa without any discontinuity in the compression of unit cell parameters, however, HP RS detected subtle discontinuous changes around 20 GPa (Manghnani et al., 2013).

HP SCXRD is a powerful tool for investigating the pressure-induced changes in the crystal structure and provides the most reliable unit cell parameter data to determine the equation of state (Angel et al., 2000; Dubrovinsky et al., 2010). With HP SCXRD, one can determine the effects of pressure on the compression of the individual coordination polyhedra, and thus examine the effects of incorporation of hydrogen associated with cationic vacancies. As a result, HP SCXRD can help us understand the mechanism of minor hydration in olivine better. Here, we report results of HP SCXRD experiments with synthetic hydrous Mg-rich olivine (Fo_{95}) to determine the effects of minor hydration associated with the Si sites on the structural evolution under compression.

2. Materials and Methods

2.1. Synthesis of olivine

The olivine used in this study was synthesized by the method of HP solid-solid reactions using a multi-anvil pressure apparatus at the Institute of Geochemistry, Chinese Academy of Sciences, Guiyang, China. The sample assembly was similar to the authors' previous study (Xu et al., 2018). In order to obtain hydrous olivine, we used an omphacite + brucite (Mg(OH)_2) mixture as the starting material. Several natural omphacite crystals with grain sizes of ~ 200 -400 μm , were selected from a crushed large eclogitic omphacite. The brucite powder was used as the water source surrounding omphacite crystals in the experimental platinum capsule. We used a Ni foil as the oxygen buffer in the synthesis (Rauch & Keppler, 2002; Xu et al., 2018). This sample assembly allowed olivine to grow at low SiO_2 activity. The sample was first compressed to 4.0

GPa over 35 minutes and then heated at 1200 °C for 30 minutes. After a run duration of 24 hours, the olivine crystals (100-400 μm size) were obtained from the quenched run product.

2.2. Chemical Analysis

Selected crystals with sizes larger than \sim 100 μm were used for electron microprobe analysis (EMPA). Analyses were conducted with a JEOL Hyperprobe JXA-8500F microscope, operating at a 15 kV accelerating voltage, 20 nA beam current, and the beam size of 10 μm . The empirical chemical formula was calculated as $\text{Mg}_{1.904\pm 9}\text{Ni}_{0.089\pm 9}\text{Fe}_{0.015\pm 3}\text{Si}_{0.991\pm 1}\text{O}_4$ based on the EMPA data (Table S1). The composition of the sample expressed in end-member molar percentages is $\text{Fo}_{95}\text{Lie}_5$, where Lie is liebenbergite ($\text{Lie, Ni}_2\text{SiO}_4$).

Analysis of water in the olivine was conducted by unpolarized FTIR measurements. We obtained two crystals without any inclusions or fractures from the quenched products for the FTIR analysis, the grain size was \sim 400 μm . The experimental details can be seen in Xu et al. (2018). The obtained FTIR spectra (Figure 1) were very similar to previous studies on synthetic olivine (Lemaire et al., 2004; Smyth et al., 2006) and indicated that the sample has four strong peaks at 3612, 3577, 3565 and 3555 cm^{-1} , and a weaker peak at 3477 cm^{-1} . These peaks can be associated with the Si site (Kohlstedt et al., 1996; Lemaire et al., 2004; Berry et al., 2005; Berry et al., 2007; Walker et al., 2007; Xue et al., 2017). Additionally, a broad peak located between 3100 and 3400 cm^{-1} confirmed that the 2H^+ for M^{2+} substitution also takes place in the synthetic olivine, but its extent is rather insignificant, relative to that at Si sites (Lemaire et al., 2004; Xue et al., 2017). The water content was estimated from integrated absorbances using the calibration of Bell et al. (2003), and the result was 1538 ppm.

2.3. Single-crystal X-ray diffraction

An olivine crystal with size ca. $40 \times 35 \times 7 \mu\text{m}$ was selected from the crushed FTIR sample, which was used for the SCXRD experiments. The sample was loaded into a short symmetric diamond anvil cell (DAC) with two Type-I diamonds (300 μm culets) mounted on Boehler-Almax-type WC seats, and this sample assembly allowed a $\pm 32^\circ$ opening angle. A rhenium gasket was indented to a thickness of \sim 40 μm by the diamond anvils, and a 180- μm sample chamber was cut using a laser drilling following indentation. Gold powder was loaded as pressure marker (Fei et al., 2007). A small ruby sphere was loaded as the pressure indicator for the gas-loading with neon (Rivers et al., 2008).

Ambient and HP SCXRD experiments were carried out with a six-circle diffractometer at the experimental station 13-BM-C of the Advanced Photon Source, Argonne National Laboratory. The experimental details can be seen in previous studies (Xu, Zhang, Dera, et al., 2017; Zhang, Dera, et al., 2017). In order to obtain precise and sufficient data to constrain the unit cell evolution with pressure, we collected the diffraction data at 40 different pressures over 0-29.9 GPa (Table S2), and at least 150 reflections (Figure 2) were used to refine the unit cell parameters at each pressure point. In addition, we collected diffraction data with increased coverage/more reflections (at least 550) with multiple detector positions at 11 different pressures for full structure determination (Table S4). The refinement of the unit cell parameters and the data reduction were completed with the GSE_ADA/RSV software package (Dera et al., 2013). Structure refinements at various pressures were carried out with SHELXL, Olex2, and VESTA software packages (Sheldrick, 2008; Dolomanov et al., 2009; Momma & Izumi, 2011). We

employed a previously reported olivine structure (Nord et al., 1982) as the initial model of the structure refinement. In the olivine structure ($M1M2TO_4$), there are two non-equivalent octahedral sites M1 and M2. According to the trend established by previous studies regarding the site preferences of transition metal ions (Burns, 1970; Nord et al., 1982), we set the M1 site as fully occupied by Mg and Ni, while M2 and T sites were fully occupied by Mg and Fe, and Si, respectively. Isotropic atomic displacement parameters (ADP) were used for all atoms, and atoms sharing the same site were assigned the same fractional coordinates and ADPs. Unit cell parameters, refinement details, atomic coordinates and ADPs, as well as calculated polyhedral parameters, including bond length and volume are listed in Tables S2-6.

3. Results and discussion

3.1. Equation of state

Upon compression, olivine retained its initial structure to the maximum pressure of 29.9(2) GPa. The unit-cell volume of olivine decreased continuously with increasing pressure over the experimental range of 0-29.9 GPa, as shown in Figure 3(a). The pressure-volume (P - V) data were fit without any constraints, using a third-order Birch-Murnaghan (BM3) equation of state (EoS) (Birch, 1947) using the program EoSFit7c (Angel et al., 2014). The obtained EoS parameters, including zero- P unit-cell volume (V_0), isothermal bulk modulus (K_{T0}), and its pressure derivative (K'_{T0}) were $V_0 = 290.46(7)$ Å³, $K_{T0} = 127.0(9)$ GPa, and $K'_{T0} = 4.46(8)$, respectively. The results indicate that the P - V data can be well described by the BM3 EoS, as shown in Figure 3(a) and the F_E - f_E plot (Figure 4(a); (Angel, 2000)).

The unit cell parameters a , b and c were also fit using a parameterized form of the BM3 EoS (Angel, 2000), the obtained axial moduli and compressibilities are shown in Table S7. From the fitted curves and F_E - f_E plots, we found that a and b can be well described by the BM3 EoS (Figure 3(b-c) and (Figure 4(b-c))). However, the fitting of the lattice parameter c was different. The compression of c exhibited softening after 20.8(1) GPa (Figure 3(d)), which was particularly pronounced in the F_E - f_E plot (Figure 4(d)). This softening phenomenon indicated that there is a change in the compression mechanism of hydrous olivine at 20.8 GPa.

Therefore, we also performed BM3 EoS fitting of data between 0 and 20.8 GPa. The results showed that the fitting of a and b within the data range of 0-20.8 GPa is highly consistent with that of fitting the whole range data (Figure 3(b-c) and (Figure 4(b-c))). The obtained axial moduli and compressibilities were also in good agreement with those derived from the whole data fitting (Table S7). However, the obtained P - c curve from fitting of the 0-20.8 GPa data significantly deviated the data above 20.8 GPa (Figure 4(d)), and the axial moduli and compressibility were drastically different from that derived from the whole data fitting (Table S7). From the perspective of unit-cell volume, the change of compression mechanism did not significantly affect the compression of olivine, as shown in Figures 3(a) and 4(a), and Table S7.

We compared our EoS results to previous HP SCXRD studies on Fo, Fa (fayalite; Fe_2SiO_4) and Lie olivine. Previous studies reported $K_{T0} = 123$ -132 GPa, and $K'_{T0} = 3.8$ -4.9 for anhydrous forsterite (Hazen, 1976; Kudoh & Takéuchi, 1985; Downs et al., 1996; Zha et al., 1998; Zhang, 1998; Finkelstein et al., 2014); $K_{T0} = 163(3)$ GPa, and $K'_{T0} = 4.5(3)$ for liebenbergite (Zhang et al., 2019); $K_{T0} = 113$ -136 GPa, and $K'_{T0} = 4.0$ -4.9 for fayalite (Hazen, 1977; Zhang, 1998; Speziale et al., 2004; Zhang, Hu, et al., 2017). Our results ($K_{T0} = 127.0(9)$ GPa, and $K'_{T0} =$

4.46(8)) were generally consistent with those for forsterite, which may imply that such minor water content and Ni have negligible effects on the bulk modulus. Additionally, previous studies on anhydrous Fo-Fa-Lie olivine did not report any changes in the compression mechanism. However, HP RS on hydrous olivine (Hushur et al., 2009; Manghnani et al., 2013) detected subtle discontinuous changes around 20 GPa, which is very close to the pressure (20.8 GPa) where we detected the softening in this study. Therefore, we attributed the *c*-axis softening after 20.8 GPa to the incorporation of water. It should be noted that the previous HP PXD study on hydrous olivine (Manghnani et al., 2013) did not observe the softening, which may indicate that HP PXD is not sufficiently sensitive to detect such a minor change in the compression mechanism.

3.1. Compressional evolution of coordination polyhedra geometry

To better understand the reasons for the change of the compression mechanism, we analyzed polyhedral evolution with pressure using the structural refinements at HP. As in previous HP studies on olivine and other mantle major minerals such as pyroxene (Zhang et al., 1997; Periotto et al., 2012; Xu, Zhang, Fan, et al., 2017), in hydrous olivine the SiO_4 tetrahedron was much more incompressible than the M1O_6 and M2O_6 octahedra (Figure 5). As shown in Figure 5, polyhedral volumes of M1O_6 and M2O_6 underwent nearly linear compression, accompanying the decrease of the unit-cell volume. However, the SiO_4 tetrahedron shrank nonlinearly and exhibited softening, particularly after 20 GPa. This softening was also indicated by the evolution of polyhedral bond lengths with pressure (Figure 6). As shown in Figure 6, the M-O bonds (M1-O and M2-O) shortened normally, just like those in anhydrous olivine and other mantle silicates like pyroxene (Zhang et al., 1997; Nestola et al., 2006; McCarthy et al., 2008; Posner et al., 2014; Zhang et al., 2016; Zhang, Hu, et al., 2017; Zhang et al., 2019). However, in the SiO_4 tetrahedron, the Si-O1 and Si-O3 bonds exhibited different degree of softening with increasing pressure, while the Si-O2 shrank normally as the M-O bonds did. The softening of the SiO_4 tetrahedron has not been reported by previous HP SCXRD studies on anhydrous olivine (Zhang, Hu, et al., 2017; Zhang et al., 2019). Posner et al. (2014) observed an increase of tetrahedral compression in pyroxene (kosmochlor) at 31 GPa, which was attributed to the stagnant kinking of the tetrahedral chain. However, this study represents a different case, as the SiO_4 tetrahedra in olivine structure are isolated and do not form any SiO_4 chains as in pyroxene minerals. Therefore, other reasons have to be responsible for the softening of the SiO_4 tetrahedron in olivine. Here, we attributed the softening to the hydration, as a reconfiguration of hydrogen sites among the Si vacancies could be induced at high pressure (Yang et al., 2019). Additionally, water has significant effects on the compression of minerals (e.g., Jacobsen, 2006) and the $\text{Si}^{4+} \leftrightarrow 4\text{H}^+$ substitution has been considered as a major mechanism by which the hydrogen can be incorporated in olivine (Kohlstedt et al., 1996; Lemaire et al., 2004; Berry et al., 2005; Berry et al., 2007; Walker et al., 2007; Balan et al., 2017; Xue et al., 2017).

4. Implications

4.1. The consequences of hydrogen incorporation on compressional behavior of olivine

The incorporation of hydrogen in olivine and its effects on the various physical and chemical properties have long been investigated (e.g., Jacobsen et al., 2008; Mao et al., 2010; Chen et al., 2011; Ghosh et al., 2013; Manghnani et al., 2013). Vibrational spectroscopy (such as infrared

spectroscopy) has been mostly employed to qualitatively and quantitatively determine the extent of incorporation of hydrogen, and the O-H vibrational bands are within the region of 3000-3700 cm^{-1} . However, the mechanisms of hydrogen incorporation, as constrained by the locations of these vibrational bands, have long been controversial. The most significant controversy has been on which mechanism accounts for the high-frequency O-H bands above 3450 cm^{-1} . Some previous studies have interpreted these bands in terms of the 2H^+ for M^{2+} substitution associated with the M vacancies, based on the cation site occupancies and polyhedral O-O edge lengths (Kudoh et al., 2006; Smyth et al., 2006; Hushur et al., 2009; Manghnani et al., 2013). However, other studies have attributed these bands to the 4H^+ for Si^{4+} substitution associated with the Si vacancies, on the basis of the compositional effects on the incorporation of water (Matveev et al., 2001; Berry et al., 2005; Berry et al., 2007; Kovács et al., 2010).

Recently, combined nuclear magnetic resonance (NMR) and vibrational spectroscopy and first-principles calculation studies have led to a conclusion that the high-frequency O-H bands above 3450 cm^{-1} in olivine are due to the 4H^+ for Si^{4+} substitution associated with the Si vacancies, which is the dominant hydration mechanism in olivine, and the 2H^+ for M^{2+} substitution associated with the M vacancies is responsible for the low-frequency ($< 3400 \text{ cm}^{-1}$) O-H bands (e.g., Balan et al., 2011; Umemoto et al., 2011; Balan et al., 2017; Xue et al., 2017). In this study, we synthesized hydrous olivine at low SiO_2 activity. In our samples, a high possibility of Si-dominant cationic vacancies could be expected, as indicated by the results of the chemical analysis (Table S1). Our FTIR spectrum of olivine (Figure 1) had the high-frequency O-H bands much more pronounced than the low-frequency bands. Therefore, the FTIR results in this study were consistent with the hydration mechanism associated with the Si.

Our HP SCXRD provide new insights into the consequences of hydrogen incorporation mechanisms in olivine at high pressure. As presented in the previous section, the polyhedral compressions of M_1O_6 and M_2O_6 behave in much the same way as normal in anhydrous olivine, while the SiO_4 tetrahedron displayed abnormal behavior, associated with softening of Si-O bonds under compression, as compared to those of anhydrous olivine (Figures 5 and 6). This softening can be explained by a reconfiguration of hydrogen sites among the Si vacancies, as indicated by the HP FTIR experiments (Yang et al., 2019). Therefore, the change in the compression mechanism of hydrous olivine at HP should be taken into account, when considering the physical properties of olivine in the mantle.

4.2. Hydration effects on the compression behavior of olivine and its HP polymorphs

This study revealed a hydration-induced compression behavior anomaly in olivine. The Si-O bonds exhibited softening with increasing pressure, which had no significant effects on the bulk compression of olivine, but caused the significant softening of the *c*-axis around 20 GPa (Figures 3-4 and 6). Recent studies on the hydration-reduced lattice thermal conductivity of olivine have suggested that under hydrous conditions, the center of a subducting slab at the transition zone would be much colder than previously expected (Chang et al., 2017). Therefore, the change in the compression behavior of hydrous olivine observed in our study may take place in a cold subducting slab, where a large volume of metastable olivine exists (e.g., Kawakatsu & Yoshioka, 2011). In such cases, the hydration-induced change in the compression anisotropy at ~ 20 GPa (Figure 6) could contribute to the seismic anisotropy of the slabs other than the lattice preferred orientation of olivine (e.g., Jung & Karato, 2001).

Under warm mantle conditions, olivine transforms to its HP polymorphs wadsleyite and ringwoodite at the transition zone, which can hold as much as 3 wt.% water (e.g., Kohlstedt et al., 1996). Therefore, a lot of studies have been conducted on the compression behavior of wadsleyite and ringwoodite (e.g., Manghnani et al., 2005; Ye et al., 2010; Ye et al., 2012; Chang et al., 2015). These studies have not reported any changes in the compression behavior of wadsleyite and ringwoodite. In wadsleyite, the H^+ is exclusively associated with its octahedral sites (e.g., Purevjav et al., 2016). However, the incorporation of hydrogen in ringwoodite is similar to that in olivine, which includes a large portion of hydrogen associated with the Si site (e.g., Ye et al., 2012; Purevjav et al., 2014). Therefore, a similar softening of the Si-O bonds and change in the compression anisotropy could be expected, as in the hydrous olivine here. Previous HP SCXRD/PXRD studies have not detected such changes (e.g., Yusa et al., 2000; Smyth et al., 2004; Manghnani et al., 2005; Ye et al., 2010; Ye et al., 2012; Chang et al., 2015), which suggests that the hydrogen incorporation mechanisms of wadsleyite and ringwoodite do not significantly change with pressure (Yang et al., 2014).

5. Conclusions

With high-quality HP SCXRD data, this study revealed a hydration-induced change in the compressional behavior of olivine at ~ 20 GPa, which was caused by the unusual softening of the Si-O bonds due to the reconfiguration of the hydrogen sites. Combining the FTIR and EMPA and HP SCXRD data, this study confirmed that the incorporation of hydrogen in olivine at low SiO_2 activity condition would be predominantly associated with the Si sites rather than the M sites. The softening of the Si-O bonds indicates a change in the hydrogen incorporation mechanism in olivine, which should be taken into account when interpreting hydration effects on the physical properties of olivine in the mantle. Wadsleyite and ringwoodite, however, do not show any softening at HP because no significant change in their hydrogen incorporation mechanism exists with pressure. The hydration-induced compression behavior change of olivine could exist in a cold subducting slab where a large volume of metastable olivine exists, and contribute to the seismic anisotropy of the slabs.

Acknowledgments

Sincere thanks go to Sergey N. Tkachev for help with gas loading. This project was funded by the National Natural Science Foundation of China (Grant Nos. 41772043, and 41802043), the Joint Research Fund in Huge Scientific Equipment (U1632112) under cooperative agreement between NSFC and CAS, the Chinese Academy of Sciences “Light of West China” Program (Dawei Fan, 2017), the Strategic Priority Research Program (B) of the Chinese Academy of Sciences (XDB 18010401), the China Postdoctoral Science Foundation (Grant No. 2018M631104), the Youth Innovation Promotion Association CAS (Dawei Fan, 2018434), the CPSF-CAS Joint Foundation for Excellent Postdoctoral Fellows (Grant No. 2017LH014). Part of this work was supported by the National Science Foundation of the United States grant 1722969. The experiments were performed at GeoSoilEnviroCARS (Sector 13), Partnership for Extreme Crystallography program (PX²), Advanced Photon Source (APS), and Argonne National Laboratory. GeoSoilEnviroCARS is supported by the National Science Foundation—Earth Sciences (EAR-1128799) and Department of Energy—Geosciences (DE-FG02-94ER14466). PX² program is supported by COMPRES under NSF Cooperative Agreement EAR 11-57758. Use of the COMPRES-GSECARS gas loading system was supported by COMPRES under NSF Cooperative Agreement EAR 11-57758 and by GSECARS. Use of the Advanced Photon Source was supported by the U.S. Department of Energy, Office of Science, Office of Basic Energy Sciences, under Contract No. DE-AC02-06CH11357. Readers can access the additional data in the supporting information.

References

Andrault, D., Bouhifd, M., Itie, J., & Richet, P. (1995). Compression and amorphization of $(\text{Mg}, \text{Fe})_2\text{SiO}_4$ olivines: an X-ray diffraction study up to 70 GPa. *Physics and Chemistry of Minerals*, 22(2), 99-107. <https://link.springer.com/article/10.1007/BF00202469>

Angel, R., Downs, R., & Finger, L. (2000). High-temperature–high-pressure diffractometry. *Reviews in mineralogy and geochemistry*, 41(1), 559-597. <https://doi.org/10.2138/rmg.2000.41.16>

Angel, R.J. (2000). Equations of state. *Reviews in mineralogy and geochemistry*, 41(1), 35-59. <https://doi.org/10.2138/rmg.2000.41.2>

Angel, R.J., Gonzalez-Platas, J., & Alvaro, M. (2014). EosFit7c and a Fortran module (library) for equation of state calculations. *Zeitschrift Fur Kristallographie*, 229(5), 405-419. <https://doi.org/10.1515/zkri-2013-1711>

Balan, E., Blanchard, M., Lazzeri, M., & Ingrin, J. (2017). Theoretical Raman spectrum and anharmonicity of tetrahedral OH defects in hydrous forsterite. *European Journal of Mineralogy*, 29(2), 201-212. <https://doi.org/10.1127/ejm/2017/0029-2599>

Balan, E., Ingrin, J., Delattre, S., Kovács, I., & Blanchard, M. (2011). Theoretical infrared spectrum of OH-defects in forsterite. *European Journal of Mineralogy*, 23(3), 285-292. <https://doi.org/10.1127/0935-1221/2011/0023-2090>

Bell, D.R., & Rossman, G.R. (1992). Water in Earth's mantle: The role of nominally anhydrous minerals. *Science*, 255(5050), 1391-1397. DOI: 10.1126/science.255.5050.1391

Bell, D.R., Rossman, G.R., Maldener, J., Endisch, D., & Rauch, F. (2003). Hydroxide in olivine: a quantitative determination of the absolute amount and calibration of the IR spectrum. *Journal of Geophysical Research: Solid Earth (1978–2012)*, 108(B2). <https://doi.org/10.1029/2001JB000679>

Beran, A., & Libowitzky, E. (2006). Water in natural mantle minerals II: Olivine, garnet and accessory minerals. *Reviews in mineralogy and geochemistry*, 62(1), 169-191. <https://doi.org/10.2138/rmg.2006.62.8>

Berry, A.J., Hermann, J., O'Neill, H.S.C., & Foran, G.J. (2005). Fingerprinting the water site in mantle olivine. *Geology*, 33(11), 869-872. <https://doi.org/10.1130/G21759.1>

Berry, A.J., O'Neill, H.S.C., Hermann, J., & Scott, D.R. (2007). The infrared signature of water associated with trivalent cations in olivine. *Earth and Planetary Science Letters*, 261(1-2), 134-142. <https://doi.org/10.1016/j.epsl.2007.06.021>

Birch, F. (1947). Finite elastic strain of cubic crystals. *Physical Review*, 71(11), 809-824. <https://doi.org/10.1103/PhysRev.71.809>

Burns, R.G. (1970). Site preferences of transition metal ions in silicate crystal structures. *Chemical Geology*, 5(4), 275-283. [http://dx.doi.org/10.1016/0009-2541\(70\)90045-8](http://dx.doi.org/10.1016/0009-2541(70)90045-8)

Chang, Y.-Y., Hsieh, W.-P., Tan, E., & Chen, J. (2017). Hydration-reduced lattice thermal conductivity of olivine in Earth's upper mantle. *Proceedings of the National Academy of Sciences*, 114(16), 4078-4081. www.pnas.org/cgi/doi/10.1073/pnas.1616216114

Chang, Y.-Y., Jacobsen, S.D., Bina, C.R., Thomas, S.-M., Smyth, J.R., Frost, D.J., et al. (2015). Comparative compressibility of hydrous wadsleyite and ringwoodite: Effect of H_2O and implications for detecting water in the transition zone. *Journal of Geophysical Research: Solid Earth*, 120(12), 8259-8280. <https://doi.org/10.1002/2015JB012123>

Chen, J., Liu, H., & Girard, J. (2011). Comparative in situ X-ray diffraction study of San Carlos olivine: Influence of water on the 410 km seismic velocity jump in Earth's mantle. *American Mineralogist*, 96(5-6), 697-702. <https://doi.org/10.2138/am.2011.3602>

Dera, P., Zhuravlev, K., Prakapenka, V., Rivers, M.L., Finkelstein, G.J., Grubor-Urosevic, O., et al. (2013). High pressure single-crystal micro X-ray diffraction analysis with GSE ADA/RSV software. *High Pressure Research*, 33(3), 466-484. <https://doi.org/10.1080/08957959.2013.806504>

Dolomanov, O.V., Bourhis, L.J., Gildea, R.J., Howard, J.A., & Puschmann, H. (2009). OLEX2: a complete structure solution, refinement and analysis program. *Journal of Applied Crystallography*, 42(2), 339-341. <https://doi.org/10.1107/S0021889808042726>

Downs, R.T., Zha, C.-S., DuFFY, T.S., & Finger, L.W. (1996). The equation of state of forsterite to 17.2 GPa and effects of pressure media. *American Mineralogist*, 81(1-2), 51-55. <https://doi.org/10.2138/am-1996-1-207>

Dubrovinsky, L., Boffa-Ballaran, T., Glazyrin, K., Kurnosov, A., Frost, D., Merlini, M., et al. (2010). Single-crystal X-ray diffraction at megabar pressures and temperatures of thousands of degrees. *High Pressure Research*, 30(4), 620-633. <https://doi.org/10.1080/08957959.2010.534092>

Duffy, T.S., Zha, C.-s., Downs, R.T., Mao, H.-k., & Hemley, R.J. (1995). Elasticity of forsterite to 16 GPa and the composition of the upper mantle. *Nature*, 378, 170-173. <https://doi.org/10.1038/378170a0>

Durben, D.J., McMillan, P.F., & Wolf, G.H. (1993). Raman study of the high-pressure behavior of forsterite (Mg_2SiO_4) crystal and glass. *American Mineralogist*, 78(11-12), 1143-1148.

Fan, D., Lu, C., Xu, J., Yan, B., Yang, B., & Chen, J. (2017). Effects of water on P - V - T equation of state of pyrope. *Physics of the Earth and Planetary Interiors*, 267, 9-18. <http://doi.org/10.1016/j.pepi.2017.03.005>

Fei, Y., Ricolleau, A., Frank, M., Mibe, K., Shen, G., & Prakapenka, V. (2007). Toward an internally consistent pressure scale. *Proceedings of the National Academy of Sciences of the United States of America*, 104(22), 9182-9186. <https://doi.org/10.1073/pnas.0609013104>

Finkelstein, G.J., Dera, P.K., Jahn, S., Oganov, A.R., Holl, C.M., Meng, Y., et al. (2014). Phase transitions and equation of state of forsterite to 90 GPa from single-crystal X-ray diffraction and molecular modeling. *American Mineralogist*, 99(1), 35-43. <https://doi.org/10.2138/am.2014.4526>

Frost, D.J., & Dolejš, D. (2007). Experimental determination of the effect of H_2O on the 410-km seismic discontinuity. *Earth and Planetary Science Letters*, 256(1-2), 182-195. <https://doi.org/10.1016/j.epsl.2007.01.023>

Ghosh, S., Ohtani, E., Litasov, K.D., Suzuki, A., Dobson, D., & Funakoshi, K. (2013). Effect of water in depleted mantle on post-spinel transition and implication for 660 km seismic discontinuity. *Earth and Planetary Science Letters*, 371, 103-111. <https://doi.org/10.1016/j.epsl.2013.04.011>

Hazen, R.M. (1976). Effects of temperature and pressure on the crystal structure of forsterite. *American Mineralogist*, 61(11-12), 1280-1293.

Hazen, R.M. (1977). Effects of temperature and pressure on the crystal structure of ferromagnesian olivine. *American Mineralogist*, 62(3-4), 286-295.

Hushur, A., Manghnani, M.H., Smyth, J.R., Nestola, F., & Frost, D.J. (2009). Crystal chemistry of hydrous forsterite and its vibrational properties up to 41 GPa. *American Mineralogist*, 94(5-6), 751-760. <https://doi.org/10.2138/am.2009.2990>

Ita, J., & Stixrude, L. (1992). Petrology, elasticity, and composition of the mantle transition zone. *Journal of Geophysical Research*, 97(B5), 6849-6866. <https://doi.org/10.1029/92JB00068>

Jacobsen, S.D. (2006). Effect of Water on the Equation of State of Nominally Anhydrous Minerals. *Reviews in Mineralogy and Geochemistry*, 62(1), 321-342. <https://doi.org/10.2138/rmg.2006.62.14>

Jacobsen, S.D., Jiang, F., Mao, Z., Duffy, T.S., Smyth, J.R., Holl, C.M., et al. (2008). Effects of hydration on the elastic properties of olivine. *Geophysical Research Letters*, 35(14), L14303. <https://doi.org/10.1029/2008GL034398>

Jung, H., & Karato, S.-i. (2001). Water-induced fabric transitions in olivine. *Science*, 293(5534), 1460-1463. DOI: 10.1126/science.1062235

Kawakatsu, H., & Yoshioka, S. (2011). Metastable olivine wedge and deep dry cold slab beneath southwest Japan. *Earth and Planetary Science Letters*, 303(1), 1-10. <https://doi.org/10.1016/j.epsl.2011.01.008>

Kirby, S., Stern, L., & Durham, W. (1991). Mantle phase changes and deep-earthquake faulting in subducting lithosphere. *Science*, 252(5003), 216-225. DOI: 10.1126/science.252.5003.216

Kirby, S.H., Stein, S., Okal, E.A., & Rubie, D.C. (1996). Metastable mantle phase transformations and deep earthquakes in subducting oceanic lithosphere. *Reviews of Geophysics*, 34(2), 261-306. <https://doi.org/10.1029/96RG01050>

Kohlstedt, D., Keppler, H., & Rubie, D. (1996). Solubility of water in the α , β and γ phases of $(\text{Mg}, \text{Fe})_2\text{SiO}_4$. *Contributions to Mineralogy and Petrology*, 123(4), 345-357. <https://doi.org/10.1007/s004100050>

Kovács, I., O'Neill, H.S.C., Hermann, J.r., & Hauri, E.H. (2010). Site-specific infrared OH absorption coefficients for water substitution into olivine. *American Mineralogist*, 95(2-3), 292-299. <https://doi.org/10.2138/am.2010.3313>

Kudoh, Y., Kurabayashi, T., Kagi, H., & Inoue, T. (2006). Cation vacancy and possible hydrogen positions in hydrous forsterite, $\text{Mg}_1.985\text{Si}0.993\text{H}0.06\text{O}_4$, synthesized at 13.5 GPa and 1300 C. *Journal of Mineralogical and Petrological Sciences*, 101(5), 265-269. <https://doi.org/10.2465/jmps.101.265>

Kudoh, Y., & Takéuchi, Y. (1985). The crystal structure of forsterite Mg_2SiO_4 under high pressure up to 149 kb. *Zeitschrift für Kristallographie-Crystalline Materials*, 171(1-4), 291-302. <https://doi.org/10.1524/zkri.1985.171.3-4.291>

Lemaire, C., Kohn, S., & Brooker, R. (2004). The effect of silica activity on the incorporation mechanisms of water in synthetic forsterite: a polarised infrared spectroscopic study. *Contributions to Mineralogy and Petrology*, 147(1), 48-57. <https://doi.org/10.1007/s00410-003-0539-x>

Litasov, K.D., Ohtani, E., Sano, A., Suzuki, A., & Funakoshi, K. (2005). Wet subduction versus cold subduction. *Geophysical research letters*, 32(13), L13312. <https://doi.org/10.1029/2005GL022921>

Liu, L.-G. (1975). Disproportionation of Ni_2SiO_4 to stishovite plus bunsenite at high pressures and temperatures. *Earth and Planetary Science Letters*, 24(3), 357-362. [https://doi.org/10.1016/0012-821X\(75\)90141-7](https://doi.org/10.1016/0012-821X(75)90141-7)

Liu, L.-G., & Mernagh, T. (1993). Raman spectra of forsterite and fayalite at high pressures and room temperature. *International Journal of High Pressure Research*, 11(5), 241-256. <https://doi.org/10.1080/08957959308203152>

Liu, W., & Li, B. (2006). Thermal equation of state of $(\text{Mg}_{0.9}\text{Fe}_{0.1})_2\text{SiO}_4$ olivine. *Physics of the Earth and Planetary Interiors*, 157(3), 188-195. <https://doi.org/10.1016/j.pepi.2006.04.003>

Manghnani, M., Amulele, G., Smyth, J., Holl, C., Chen, G., Prakapenka, V., et al. (2005). Equation of state of hydrous Fo90 ringwoodite to 45 GPa by synchrotron powder diffraction. *Mineralogical Magazine*, 69(3), 317-323. <https://doi.org/10.1180/0026461056930253>

Manghnani, M.H., Hushur, A., Smyth, J.R., Nestola, F., Dera, P., Sekar, M., et al. (2013). Compressibility and structural stability of two variably hydrated olivine samples (Fo₉₇Fa₃) to 34 GPa by X-ray diffraction and Raman spectroscopy. *American Mineralogist*, 98(11-12), 1972-1979. <https://doi.org/10.2138/am.2013.4462>

Mao, H., Takahashi, T., & Bassett, W.A. (1970). Isothermal compression of the spinel phase of Ni_2SiO_4 up to 300 kilobars at room temperature. *Physics of the Earth and Planetary Interiors*, 3, 51-53. [https://doi.org/10.1016/0031-9201\(70\)90043-9](https://doi.org/10.1016/0031-9201(70)90043-9)

Mao, Z., Fan, D.W., Lin, J.F., Yang, J., Tkachev, S.N., Zhuravlev, K., et al. (2015). Elasticity of single-crystal olivine at high pressures and temperatures. *Earth and Planetary Science Letters*, 426, 204-215. <https://doi.org/10.1016/j.epsl.2015.06.045>

Mao, Z., Jacobsen, S., Jiang, F., Smyth, J., Holl, C., Frost, D., et al. (2010). Velocity crossover between hydrous and anhydrous forsterite at high pressures. *Earth and Planetary Science Letters*, 293(3-4), 250-258. <https://doi.org/10.1016/j.epsl.2010.02.025>

Mao, Z., & Li, X. (2016). Effect of hydration on the elasticity of mantle minerals and its geophysical implications. *Science China Earth Sciences*, 59(5), 873-888. <https://doi.org/10.1007/s11430-016-5277-9>

Matveev, S., O'neill, H.S.C., Ballhaus, C., Taylor, W.R., & Green, D. (2001). Effect of silica activity on OH⁻ IR spectra of olivine: implications for low- αSiO_2 mantle metasomatism. *Journal of Petrology*, 42(4), 721-729. <https://doi.org/10.1093/petrology/42.4.721>

McCarthy, A.C., Downs, R.T., Thompson, R.M., & Redhammer, G.J. (2008). In situ high-pressure single-crystal X-ray study of aegirine, $\text{NaFe}^{3+}\text{Si}_2\text{O}_6$, and the role of M1 size in clinopyroxene compressibility. *American Mineralogist*, 93(11-12), 1829-1837. <https://doi.org/10.2138/am.2008.2725>

Momma, K., & Izumi, F. (2011). VESTA 3 for three-dimensional visualization of crystal, volumetric and morphology data. *Journal of Applied Crystallography*, 44(6), 1272-1276. <https://doi.org/10.1107/S0021889811038970>

Mosenfelder, J.L., Deligne, N.I., Asimow, P.D., & Rossman, G.R. (2006). Hydrogen incorporation in olivine from 2-12 GPa. *American Mineralogist*, 91(2-3), 285-294. <https://doi.org/10.2138/am.2006.1943>

Nestola, F., Gatta, G.D., & Ballaran, T.B. (2006). The effect of Ca substitution on the elastic and structural behavior of orthoenstatite. *American Mineralogist*, 91(5-6), 809-815. <https://doi.org/10.2138/am.2006.1982>

Nestola, F., Pasqual, D., Smyth, J., Novella, D., Secco, L., Manghnani, M., et al. (2011). New accurate elastic parameters for the forsterite-fayalite solid solution. *American Mineralogist*, 96(11-12), 1742-1747. <https://doi.org/10.2138/am.2011.3829>

Nord, A.G., Annersten, H., & Filippidis, A. (1982). The cation distribution in synthetic Mg-Fe-Ni olivines. *American Mineralogist*, 67(11-12), 1206-1211.

Periotto, B., Balić-Žunić, T., Nestola, F., Katerinopoulou, A., & Angel, R.J. (2012). Re-investigation of the crystal structure of enstatite under high-pressure conditions. *American Mineralogist*, 97(10), 1741-1748. <https://doi.org/10.2138/am.2012.4157>

Posner, E.S., Dera, P., Downs, R.T., Lazarz, J.D., & Irmenn, P. (2014). High-pressure single-crystal X-ray diffraction study of jadeite and kosmochlor. *Physics and Chemistry of Minerals*, 41(9), 695-707. <https://doi.org/10.1007/s00269-014-0684-y>

Purevjav, N., Okuchi, T., Tomioka, N., Abe, J., & Harjo, S. (2014). Hydrogen site analysis of hydrous ringwoodite in mantle transition zone by pulsed neutron diffraction. *Geophysical Research Letters*, 41(19), 6718-6724. <https://doi.org/10.1002/2014GL061448>

Purevjav, N., Okuchi, T., Tomioka, N., Wang, X., & Hoffmann, C. (2016). Quantitative analysis of hydrogen sites and occupancy in deep mantle hydrous wadsleyite using single crystal neutron diffraction. *Scientific Reports*, 6, 34988. <https://doi.org/10.1038/srep34988>

Rauch, M., & Keppler, H. (2002). Water solubility in orthopyroxene. *Contributions to Mineralogy and Petrology*, 143(5), 525-536. <https://doi.org/10.1007/s00410-002-0365-6>

Ringwood, A.E. (1991). Phase transformations and their bearing on the constitution and dynamics of the mantle. *Geochimica et Cosmochimica Acta*, 55(8), 2083-2110. [https://doi.org/10.1016/0016-7037\(91\)90090-R](https://doi.org/10.1016/0016-7037(91)90090-R)

Rivers, M., Prakapenka, V.B., Kubo, A., Pullins, C., Holl, C.M., & Jacobsen, S.D. (2008). The COMPRES/GSECARS gas-loading system for diamond anvil cells at the Advanced Photon Source. *High Pressure Research*, 28(3), 273-292. <https://doi.org/10.1080/08957950802333593>

Rouquette, J., Kantor, I., McCammon, C., Dmitriev, V., & Dubrovinsky, L. (2008). High-pressure studies of $(\text{Mg}_{0.9}\text{Fe}_{0.1})_2\text{SiO}_4$ olivine using Raman spectroscopy, X-ray diffraction, and Mössbauer spectroscopy. *Inorganic Chemistry*, 47(7), 2668-2673. <https://pubs.acs.org/doi/abs/10.1021/ic701983w>

Santamaria-Perez, D., Thomson, A., Segura, A., Pellicer-Torres, J., Manjon, F.J., Corà, F., et al. (2016). Metastable structural transformations and pressure-induced amorphization in natural $(\text{Mg}, \text{Fe})_2\text{SiO}_4$ olivine under static compression: A Raman spectroscopic study. *American Mineralogist*, 101(7), 1642-1650. <https://doi.org/10.2138/am-2016-5389CCBY>

Sheldrick, G.M. (2008). A short history of SHELX. *Acta Crystallogr A*, 64(Pt 1), 112-22. <https://doi.org/10.1107/S0108767307043930>

Smyth, J.R., Frost, D.J., Nestola, F., Holl, C.M., & Bromiley, G. (2006). Olivine hydration in the deep upper mantle: Effects of temperature and silica activity. *Geophysical Research Letters*, 33(15). <https://doi.org/10.1029/2006GL026194>

Smyth, J.R., Holl, C.M., Frost, D.J., & Jacobsen, S.D. (2004). High pressure crystal chemistry of hydrous ringwoodite and water in the Earth's interior. *Physics of the Earth and Planetary Interiors*, 143, 271-278. <https://doi.org/10.1016/j.pepi.2003.08.011>

Speziale, S., Duffy, T.S., & Angel, R.J. (2004). Single-crystal elasticity of fayalite to 12 GPa. *Journal of Geophysical Research: Solid Earth*, 109(B12). <https://doi.org/10.1029/2004JB003162>

Umemoto, K., Wentzcovitch, R.M., Hirschmann, M.M., Kohlstedt, D.L., & Withers, A.C. (2011). A first-principles investigation of hydrous defects and IR frequencies in forsterite: The case for Si vacancies. *American Mineralogist*, 96(10), 1475-1479. <https://doi.org/10.2138/am.2011.3720>

Walker, A.M., Hermann, J., Berry, A.J., & O'Neill, H.S.C. (2007). Three water sites in upper mantle olivine and the role of titanium in the water weakening mechanism. *Journal of Geophysical Research-Solid Earth*, 112(B5). <https://doi.org/10.1029/2006JB004620>

Will, G., Hoffbauer, W., Hinze, E., & Lauterjung, J. (1986). The compressibility of forsterite up to 300 kbar measured with synchrotron radiation. *Physica B+C*, 139, 193-197. [https://doi.org/10.1016/0378-4363\(86\)90556-5](https://doi.org/10.1016/0378-4363(86)90556-5)

Xu, J., Zhang, D., Dera, P., Zhang, B., & Fan, D. (2017). Experimental evidence for the survival of augite to transition zone depths, and implications for subduction zone dynamics. *American Mineralogist*, 102(7), 1516-1524. <https://doi.org/10.2138/am-2017-5959>

Xu, J., Zhang, D., Fan, D., Downs, R.T., Hu, Y., & Dera, P. (2017). Isosymmetric pressure-induced bonding increase changes compression behavior of clinopyroxenes across jadeite-aegirine solid solution in subduction zones. *Journal of Geophysical Research: Solid Earth*, 122(1), 142-157. <https://doi.org/10.1002/2016JB013502>

Xu, J., Zhang, D., Fan, D., Zhang, J.S., Hu, Y., Guo, X., et al. (2018). Phase Transitions in Orthoenstatite and Subduction Zone Dynamics: Effects of Water and Transition Metal Ions. *Journal of Geophysical Research: Solid Earth*, 123(4), 2723-2737. <https://doi.org/10.1002/2017JB015169>

Xue, X., Kanzaki, M., Turner, D., & Loroch, D. (2017). Hydrogen incorporation mechanisms in forsterite: New insights from ^{1}H and ^{29}Si NMR spectroscopy and first-principles calculation. *American Mineralogist*, 102(3), 519-536. <https://doi.org/10.2138/am-2017-5878>

Yang, X., Keppler, H., Dubrovinsky, L., & Kurnosov, A. (2014). In-situ infrared spectra of hydroxyl in wadsleyite and ringwoodite at high pressure and high temperature. *American Mineralogist*, 99(4), 724-729. <https://doi.org/10.2138/am.2014.4634>

Yang, Y., Liu, W., Qi, Z., Wang, Z., Smyth, J.R., & Xia, Q. (2019). Re-configuration and interaction of hydrogen sites in olivine at high temperature and high pressure. *American Mineralogist*, Accepted. <https://doi.org/10.2138/am-2019-6921>

Ye, Y., Brown, D.A., Smyth, J.R., Panero, W.R., Jacobsen, S.D., Chang, Y.-Y., et al. (2012). Compressibility and thermal expansion of hydrous ringwoodite with 2.5(3) wt% H_2O . *American Mineralogist*, 97(4), 573-582. <https://doi.org/10.2138/am.2012.4010>

Ye, Y., Smyth, J.R., Hushur, A., Manghnani, M.H., Lonappan, D., Dera, P., et al. (2010). Crystal structure of hydrous wadsleyite with 2.8% H₂O and compressibility to 60 GPa. *American Mineralogist*, 95(11-12), 1765-1772. <https://doi.org/10.2138/am.2010.3533>

Yusa, H., Inoue, T., & Ohishi, Y. (2000). Isothermal compressibility of hydrous ringwoodite and its relation to the mantle discontinuities. *Geophysical Research Letters*, 27(3), 413-416. <https://doi.org/10.1029/1999GL011032>

Zha, C.-S., Duffy, T.S., Downs, R.T., Mao, H.-K., & Hemley, R.J. (1998). Brillouin scattering and X-ray diffraction of San Carlos olivine: direct pressure determination to 32 GPa. *Earth and Planetary Science Letters*, 159(1), 25-33. [https://doi.org/10.1016/S0012-821X\(98\)00063-6](https://doi.org/10.1016/S0012-821X(98)00063-6)

Zha, C.-S., Duffy, T.S., Downs, R.T., Mao, H.K., & Hemley, R.J. (1996). Sound velocity and elasticity of single - crystal forsterite to 16 GPa. *Journal of Geophysical Research*, 101(B8), 17535-17545. <https://doi.org/10.1029/96JB01266>

Zhang, D., Dera, P.K., Eng, P.J., Stubbs, J.E., Zhang, J.S., Prakapenka, V.B., et al. (2017). High Pressure Single Crystal Diffraction at PX². *Journal of visualized experiments: JoVE*(119), e54660. <https://www.jove.com/video/54660>

Zhang, D., Hu, Y., & Dera, P.K. (2016). Compressional behavior of omphacite to 47 GPa. *Physics and Chemistry of Minerals*, 43(10), 707-715. <https://doi.org/10.1007/s00269-016-0846-1>

Zhang, D., Hu, Y., Xu, J., Downs, R.T., Hammer, J.E., & Dera, P.K. (2019). High-pressure behavior of liebenbergite: The most incompressible olivine-structured silicate. *American Mineralogist*, 104(4), 580-587. <https://doi.org/10.2138/am-2019-6680>

Zhang, J.S., Hu, Y., Shelton, H., Kung, J., & Dera, P. (2017). Single-crystal X-ray diffraction study of Fe₂SiO₄ fayalite up to 31 GPa. *Physics and Chemistry of Minerals*, 44(3), 171-179. <https://doi.org/10.1007/s00269-016-0846-1>

Zhang, L. (1998). Single crystal hydrostatic compression of (Mg, Mn, Fe, Co)₂SiO₄ olivines. *Physics and chemistry of minerals*, 25(4), 308-312. <https://doi.org/10.1007/s002690050>

Zhang, L., Ahsbahs, H., Hafner, S.S., & Kutoglu, A. (1997). Single-crystal compression and crystal structure of clinopyroxene up to 10 GPa. *American Mineralogist*, 82(3), 245-258. <https://doi.org/10.2138/am-1997-3-402>

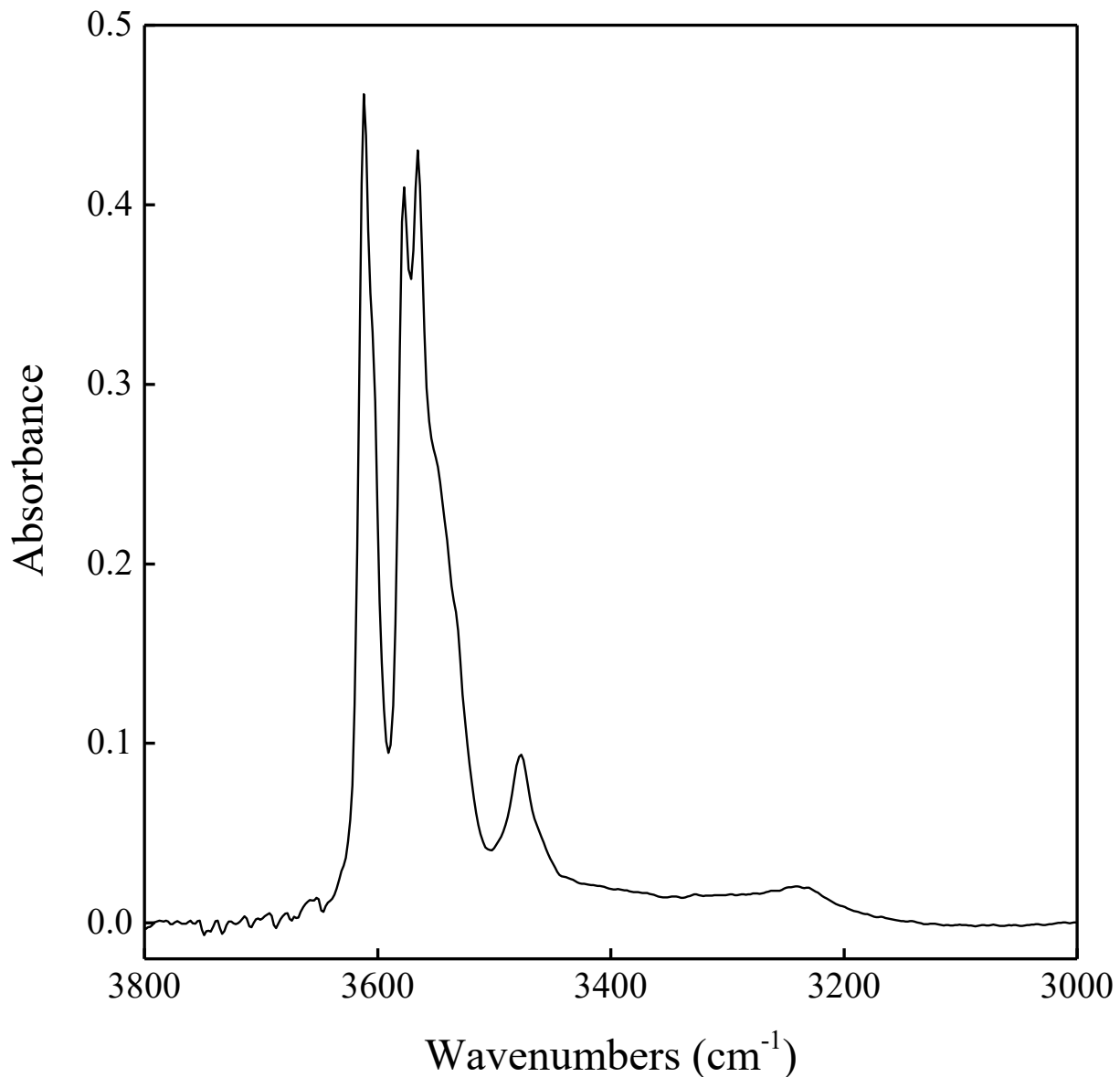


Figure 1. Selected unpolarized FTIR spectra of hydrous olivine synthesized at 4 GPa and 1250 °C. Integration of the spectrum indicates an H₂O content of 1538 ppm.

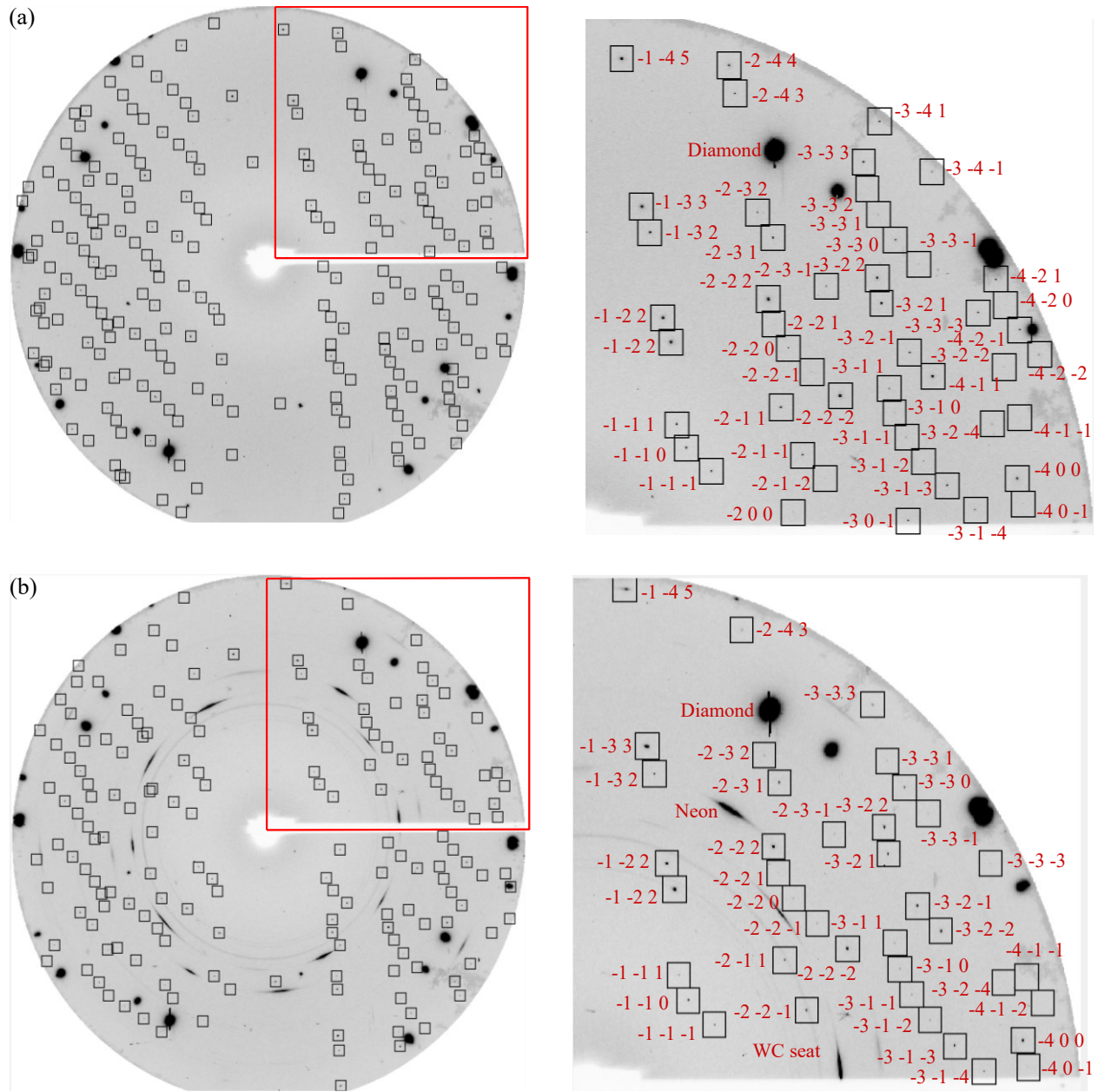


Figure 2. Single crystal X-ray diffraction patterns of hydrous olivine at (a). $P = 1.2(1)$ GPa and (b) $P = 29.9(2)$ GPa.

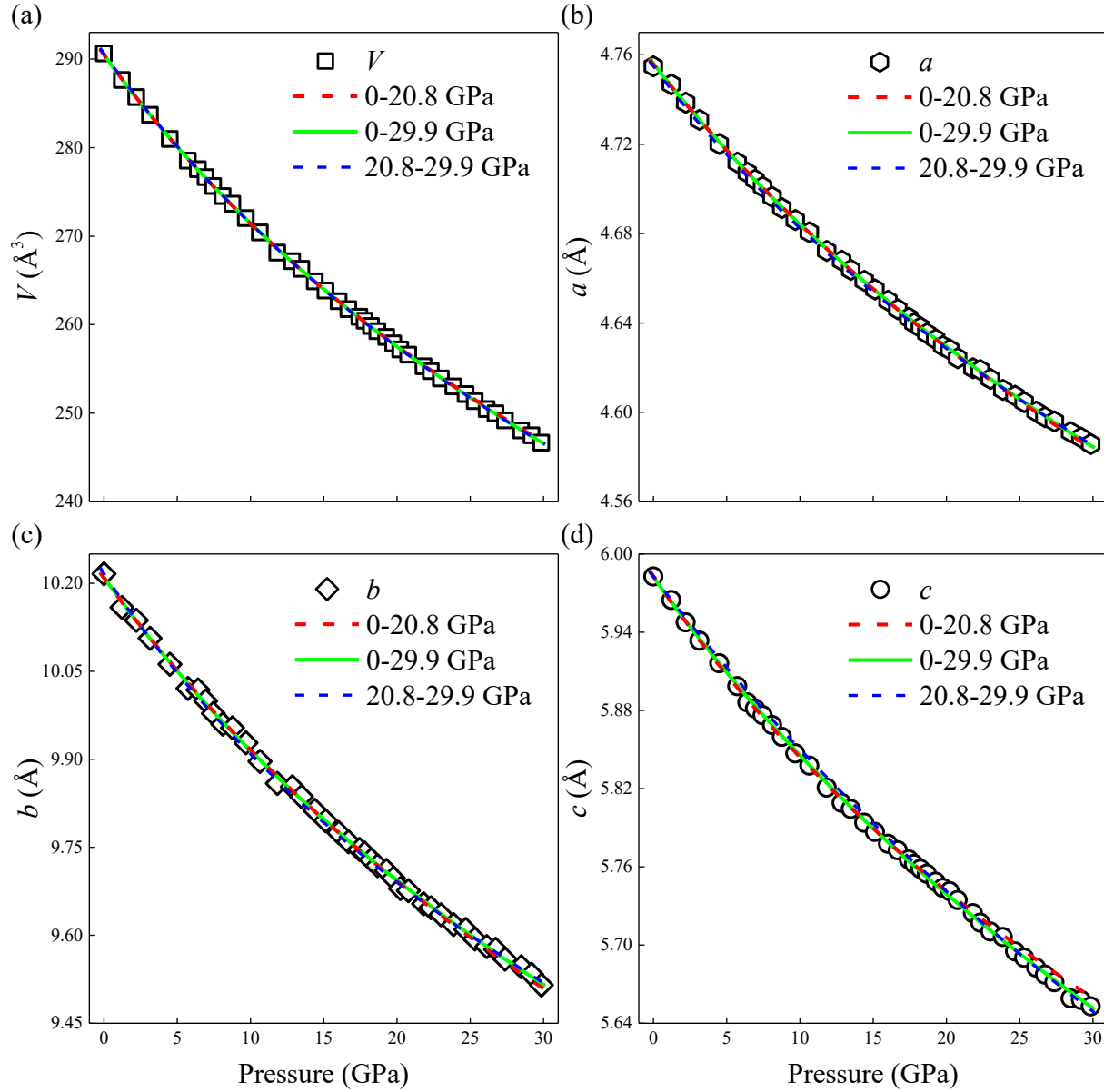


Figure 3. Evolution of the lattice parameters as a function of pressure: (a) V , (b) a , (c) b , and (d) c . The solid line represents the BM3 EoS fitting based on all data of this study, and the dashed line is the BM3 EoS-fitting curve based on data of 0-20.8 GPa. The error bars are smaller than the symbols in this study.

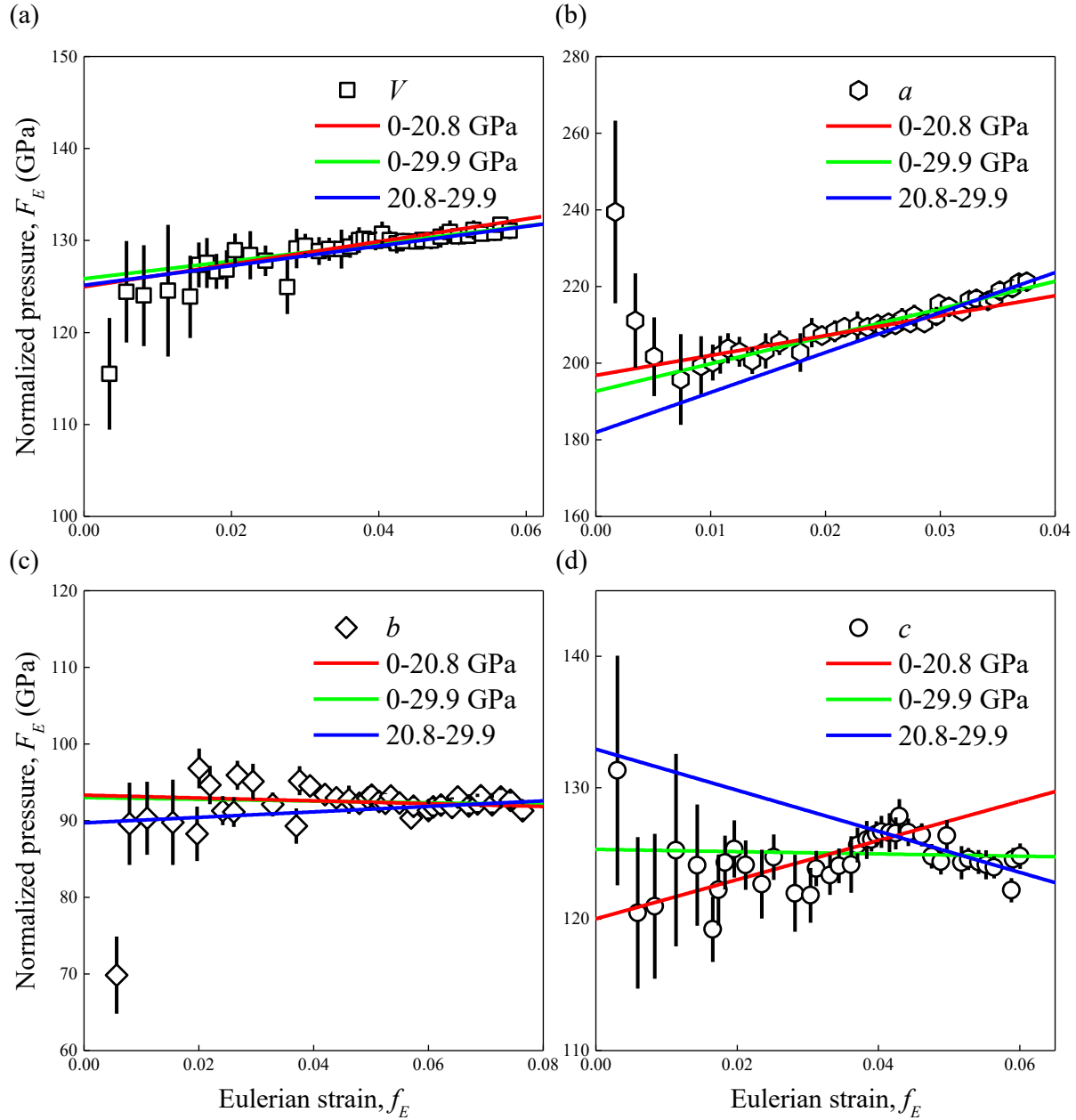


Figure 4. Eulerian strain-normalized pressure (F_E-f_E) plot (Angel, 2000) of the V (a) a (b), b (c), and c (d) of hydrous olivine. The green solid straight line represents a linear fit of all the F_E-f_E data, and the red straight line represents a linear fit of the F_E-f_E data of 0-20.8 GPa.

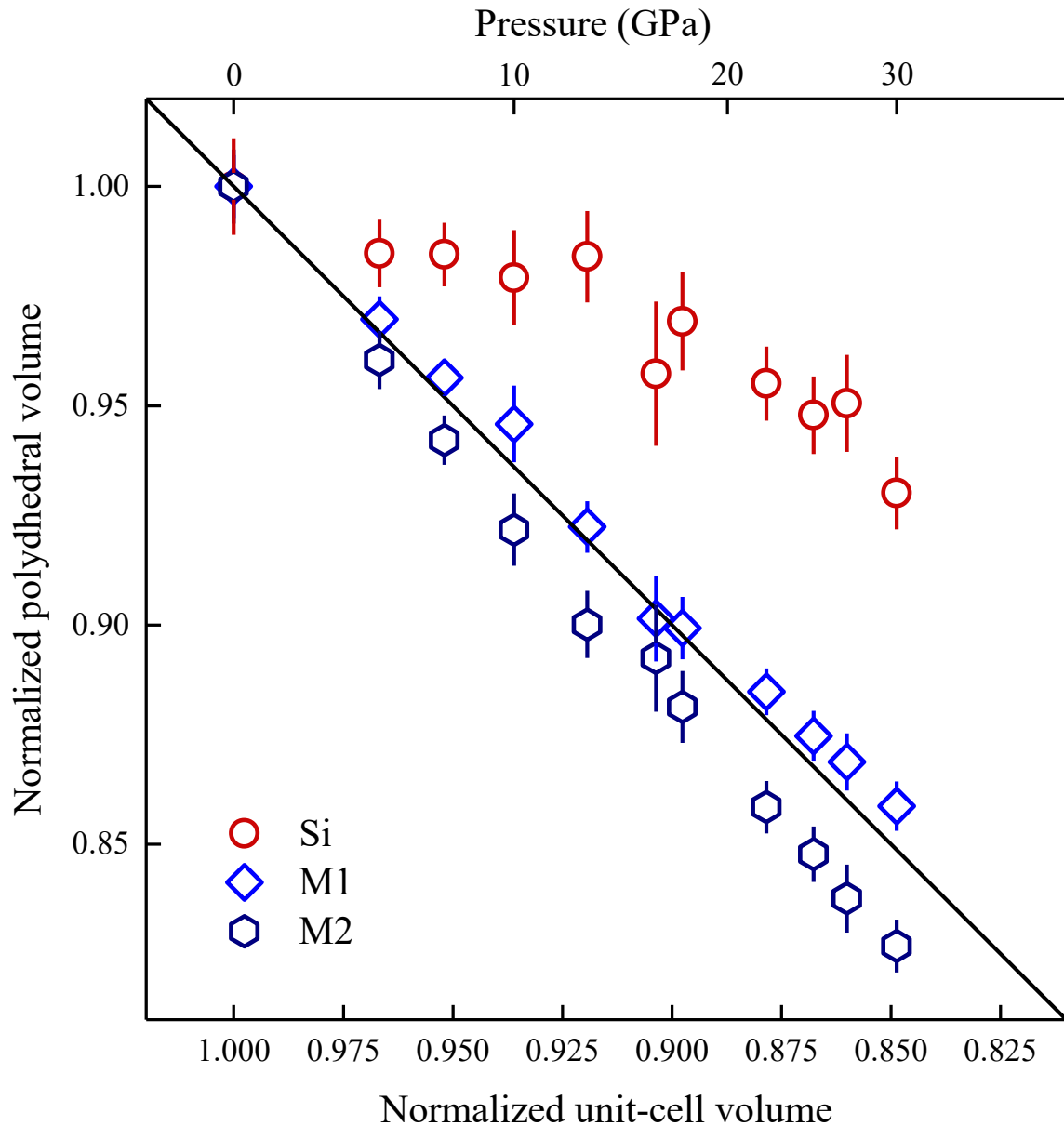


Figure 5. Normalized polyhedral volume as a function of a normalized unit-cell volume at different pressures. The black dotted line represents the $y = x$ line. The error bars were calculated using the method described by Zhang et al. (2019).

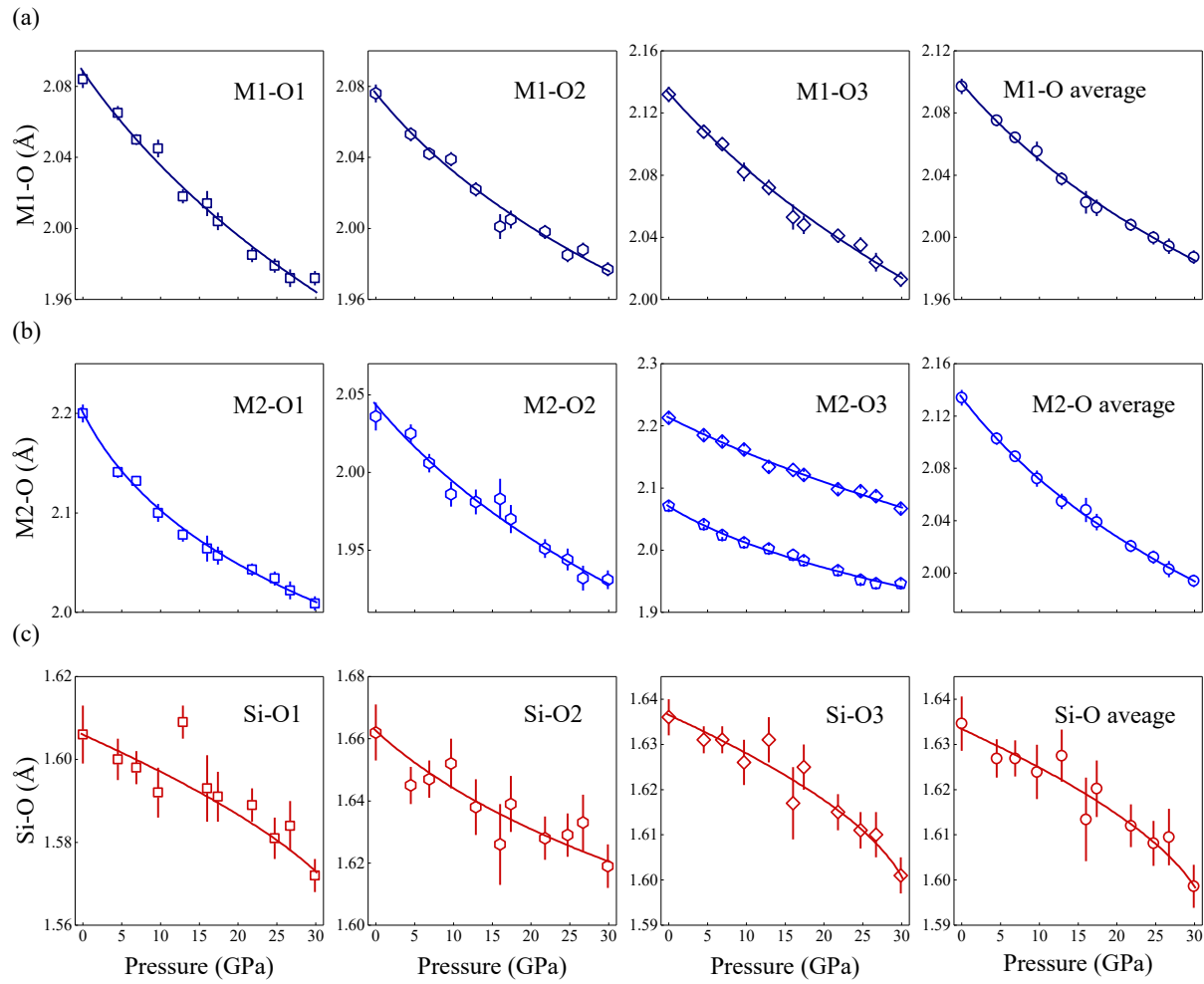


Figure 6. Pressure dependence of polyhedral bond lengths: (a) M1-O, (b) M2-O and (c) Si-O. The solid line represents a BM3 fitting of the whole range data.

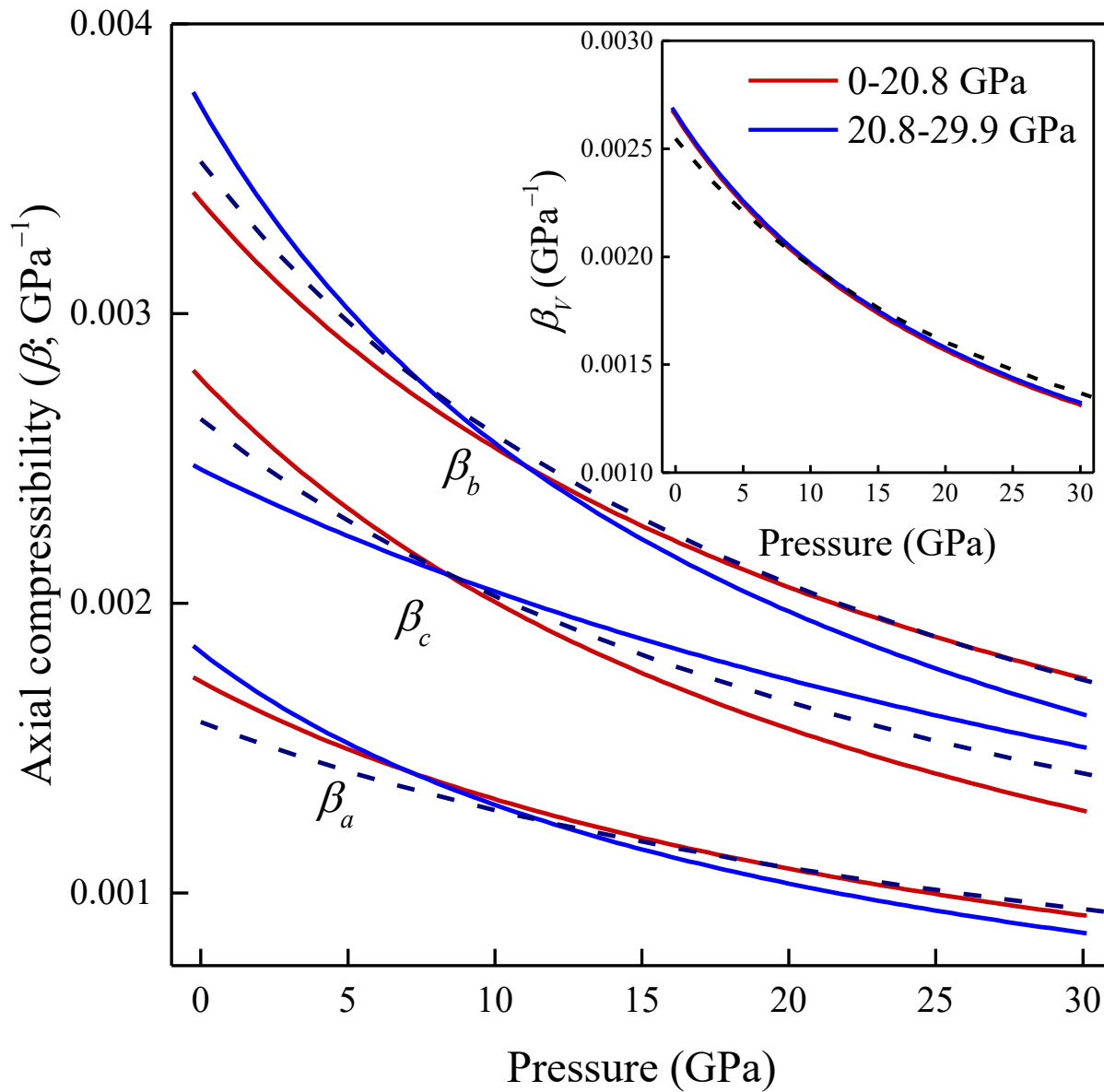


Figure 7. Pressure dependences of axial compressibility (β_a, β_b , and β_c), and the insert figure shows the data of the bulk compressibility (β_V). The dashed lines represent the anhydrous forsterite (Finkelstein et al., 2014), and the solid lines show the hydrous olivine data in this study.